# Hybrid RANS/LES Investigation of Precessing Vortex Core (PVC) in a Swirl Premixed Combustor

Zakaria Mansouri[1,2], Toufik Boushaki[2,*]
[1]Laboratory of Mechanics, Amar Telidji University, Laghouat, Algeria
[2]ICARE, CNRS, Avenue de la Recherche Scientifique, 45071 Orléans Cedex 2, France

## 1 Introduction

Swirling flows are commonly used in modern gas turbine combustors to promote the stabilization of flames and reduce pollutant emissions. Vortex breakdown that presents near the burner exit is a unique feature that characterizes the swirling flow. It leads to the formation of a central recirculation zone (CRZ), which puts the burned gases and the unburned reactants in a permanent mixing. The CRZ is commonly associated with stagnation points and those often accompanied by the occurrence of coherent precessing vortex core (PVC). The PVC is characterized by its precessing around the symmetry axis of the burner [1]. Various studies have been conducted to investigate the effect of PVC on the stabilization of swirling flames [2-4]. Numerous experimental [5-7] and numerical [8-10] studies were investigated swirling flows features at an isothermal condition. Bulat et al. [8] performed a computational study of isothermal confined swirling flow in an industrial gas turbine combustor using Large Eddy Simulation (LES). Their isothermal LES results were found to be in good agreement with experimental data. They observed two separate structures inside the combustor: PVC and a central vortex core (CVC). The two large scale flow features correspond to three-dimensional vortex structures with long lifetimes. The PVC found to be to a double helical and he CVC is formed at the tail end of the CRZ. Zhang et al. [9] studied the non-reacting unconfined flow fields with and without swirl of a Cambridge swirl burner using LES. Their results show that the annular swirling flow has a minor impact on the formation of the bluff-body recirculation zone. They observed that the formed 3D vortex structures near the shear layers, display ring structures in non-swirling flow and helical structures in swirling flow near the burner exit. The analysis of the helical structures reveals that flow fields contain co-existing helical and toroidal shaped coherent structures. The helical structure is associated with the PVC and it's the most energetic dynamic flow structure. In this paper, Detached Eddy Simulation (DES) is performed to analyses the high turbulent swirling flow in a model vortex burner of Fernandes et al. [5]. The study scrutinizes the ability of DES to capture highly unsteady flow features and precessing coherent structures inside such vortex burner. In this analyze, the mean flow and the unsteady flow with its features are investigated. In addition, a particular attention is given to the PVC present in the expansion plane of the burner.

*Correspondence to: toufik.boushaki@cnrs-orleans.fr 

## 2 Sample Experimental Setup

The model vortex burner [14] used in this work consists of a swirl generator with variable blade angles to control the degree of swirl (Figure 1.a). To discharge into the combustion chamber (CC), the swirling flow passes through a premixing tube (PT). Liquid fuel (Jet-A1) can be introduced through an atomizer positioned on the centerline of the PT, as reported by Anacleto et al. [11]. Gaseous fuel (Propane) is used as a substitute for jet fuel and is injected upstream of the PT. The premixing tube ends with a contraction from a diameter of 40 mm to D = 50 mm. The CC is made of cylindrical stainless steel ducts with an inner diameter of 110 mm and a total length of 300 mm. Inside the burner, average velocity and precession frequency were $U_0$ = 30 m/s and $f$ = 420 Hz are corresponding to Re = $8\times10^4$. During the experiments, a high swirl number equal to 1.05 is used and corresponds to the swirler blade angel 50°.

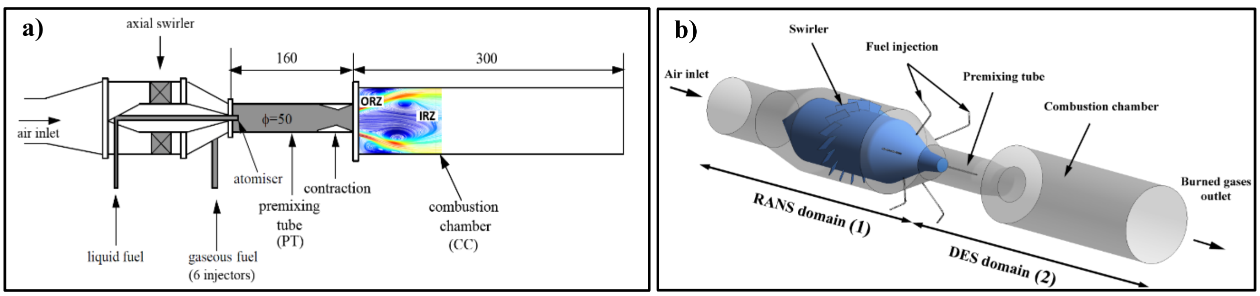


Figure 1. Schematic diagram of the experimental combustor (a) and computational domain (b)

## 3 Computational Details

ANSYS-Fluent 14 CFD software is used for the simulations. It uses the finite-volume method to solve the governing equations. The continuity and Navier–Stokes governing equations for compressible flow are ensemble averaged (URANS) near-wall regions and filtered (LES) in the rest of the flow using DES hybrid model. The details of the used DES strategy can be found in Strelets [13]. The computational domain presented in Figure 1.b is divided in tow sub-domains. The first covers the air inlet, the swirl generator and the fuel injection duct. The second covers the premixing tube including the contraction and a fraction of the atmosphere at the burner exit. Note that the CC is not included to the domain in order to respect the unconfined condition. The present DES computations focus on the second sub-domain which contains the highly unsteady flow features and precessing coherent structures. Therefore, the first sub-domain is simulated using RANS strategy in order to generate realistic inlet boundary conditions to initialize the flow in the second sub-domain and avoid the constant uniform inlet velocities. The multi-block technique is used to generate a structured grid. The studied second sub-domain consists of 35 blocks and contains 3 million hexahedral grid cells. The suitable minimum grid spacing in x, y and z directions is calculated accordingly to the estimated Taylor turbulent microscale $\lambda \sim D/72$ in regions of potential turbulence generation and large velocity gradients. The used adjusted grid spacing gives a satisfactory results and good agreement with experimental data, as documented by Mansouri et al. [14].

## 4 Results and Discussion

### 4.1 Time averaged and instantaneous flow fields

Figure 3.a presents the two-dimensional averaged flow field on the streamwise plane through the vortex burner, using streamline patterns colored by averaged axial velocity (with $U_0$=30 m/s). The sudden expansion of the flow at the burner exit induces two recirculation zones, as expected from a turbulent swirling flow. The first, CRZ is cone-shaped reverse flow stream extending from the burner exit along the axial direction as result of vortex breakdown. The second, ORZ is formed at the plane wall of the burner due to its geometry which the swirling jet encounters when expands. It is shown that the sudden expansion induces also strong velocity gradients up to $1.1U_0$. Figure 3.b shows the two-dimensional instantaneous flow field on the streamwise plane through the vortex burner, using streamline patterns colored by instantaneous axial velocity. It is clearly shown that the instantaneous flow field contains specific features that are not present in the averaged flow field. The most specific features compared to the averaged flow field are the vortices in the ISL marked by black arrows, which are arranged as a zig-zag marked by white dashed line. This arrangement informs the existing of a helical 3D coherent vortex in the ISL. The helical vortex is known as the Precessing Vortex Core (PVC). Another features locate in the ISL of the instantaneous flow field are associated frontally to the vortices of the ISL, such as the stagnation points marked by red dots. They formed as a result of the collision between the arrangements of vortices in the ISL. The vortices in the OSL are particular features that relevant to the present flow field.

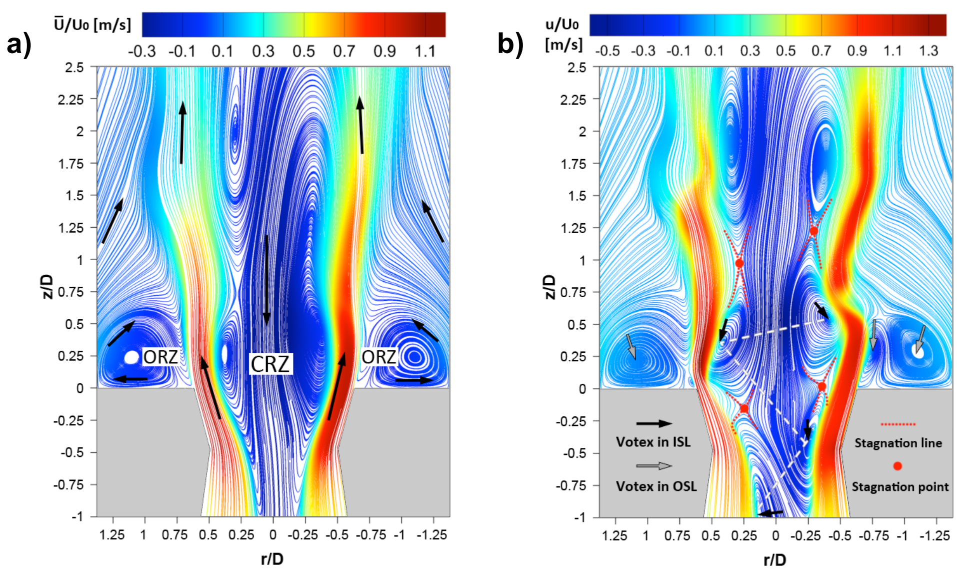


Figure 3. The streamline patterns of the averaged (a) and instantaneous (b) flow fields

## 4.2 Validation with experimental measurements

Figure 4 illustrates comparisons between LDV measurements [11] and present predicted averaged axial (a) and averaged swirling (b) velocity profiles close to the expansion zone at z = 0.25D. In Figure 6.a, the present DES strategy could be capable of capturing the averaged flow field structures. This is clearly seen close to the burner center (r/D = 0), where the negative values present the CRZ and also close to r/D = 0.5 where the velocity peak present the shear layer between the IRZ and the ORZ. Meanwhile, in Figure 6.b the DES results show the same tend of the averaged swirling velocity profile with the exact values between r/D = 0 and r/D = 0.5 and close to r/D = 1 too. Moreover, the predictions of the radial profiles of the both velocities are all in good agreement with experimental measurements. Far of the expansion zone (z/D = 1.75), additional profiles of both averaged velocities are presented. This gives an idea about the flow structure in this region. The flow starts to be weak and the velocity peaks are decreased around 50% (about 0.5 $U_0$) comparing with the validation location.

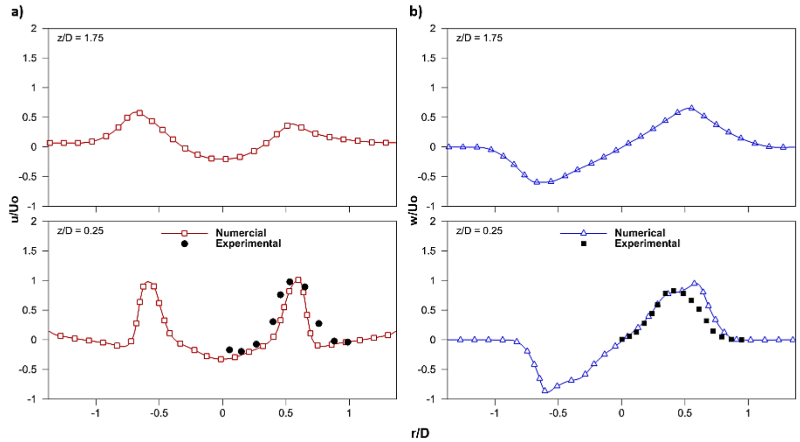


Figure 4. Radial profiles of averaged axial (a) and averaged swirling (b) velocities.

### 4.3 Phase-angle analysis of the flow field

In Figure 5 the instantaneous flow field along the streamwise plane of the burner is extensively analyzed using the phase-angle technique. The flow field is characterized using streamline patterns at four phase angles φ = 0°, 45°, 90° and 135°. The stagnation points in the flow marked by red dots are linked with blue lines, in order to follow their manifestation at each phase angle. At φ = 0°, six stagnation points occurred in the flow and link the vortices. Four of them associate the vortices in the ISL and two associate the vortices in the OSL. The flow structure shows a difference at φ = 45° with new revealed stagnation points (at around z/D = -1 and z/D = 1.75) in both ISL and OSL. Additional stagnation point is appeared in the OSL as a result of the interaction between the entrained free flow and the OSL, it locates at around z/D = 0.75.

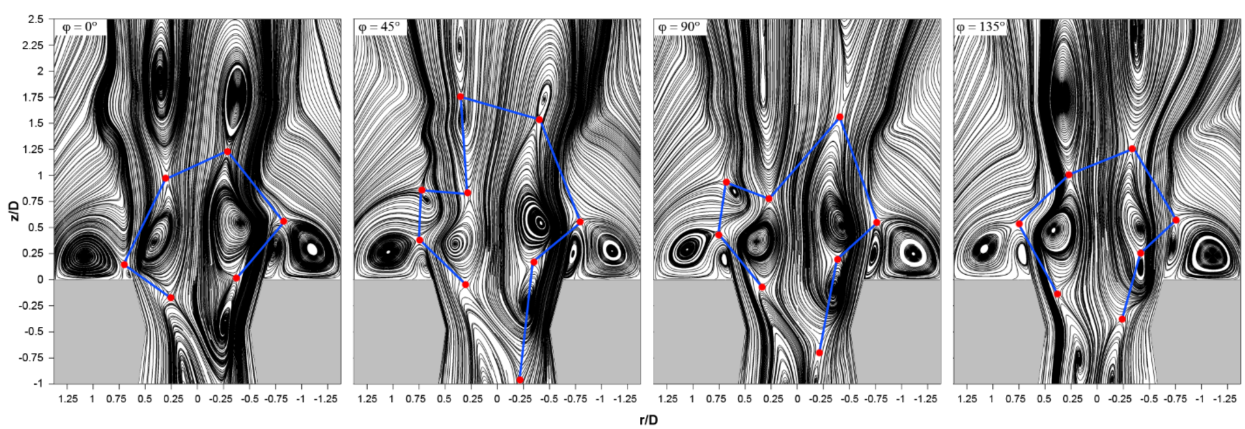


Figure 5. Phase angles of the instantaneous flow field.

Moreover, at φ = 90° one point in the ISL is disappeared and the positions of the other points almost stay the same and no considerable difference is observed, except the point in the contraction section which is moved forward by around 0.25D compared with its last position at φ = 45°. At the last phase angle φ = 135°, the flow structure differed considerably comparing with the two previous angles, and it tends to have the same positions of the stagnation points as at the initial phase angle φ = 0°. Finally, the results demonstrate the high unsteady features of the turbulent swirling flow that are strongly associated with PVC.

### 4.4 Precessing Vortex Core

Figure 6.a shows an instantaneous view of the PVC using a low pressure isosurface colored by instantaneous axial velocity. It can be seen that in the contraction section, the instability sets on and the PVC is formed taking on a helical shape. The direction of the resulting precession is the direction of the swirler itself. It is desirable to determine some parameters for the PVC, such as the vortex radius R and its corresponding velocity u(R). Figure 6.b presents vectors of the flow fields in two slices perpendicular to the vortex axis. The vortex centerlines (marked with the dashed black line) with velocity gradient from high at the left to low at the right in the primary slice with the inversion of this gradient in the secondary slice, can be seen. The axial velocity profiles across the vortex centerlines are plotted in Figure 6.c. The profiles of both slices show that the vortex is limited by its maximum and minimum circumferential velocity u(R). The locations of the circumferential velocity limits of the vortex and the zero velocity at the vortex center, defines the PVC radius R. The minimum and maximum u(R) with corresponding R characterize the coherent-body rotation of the PVC. By taking the case of the secondary slice profile, the minimum u(R) = -0.23 locates at r/D = 0.33 and the maximum u(R) = 1.05 locates at r/D = 0.59. This indicates that the coherent-body exhibits a non-symmetric rotation around the axis of the vortex. Indeed, it can be seen that the rotation center locates at r/D = 0.42, which does not correspond to the average value between the minimum and maximum u(R) locations.

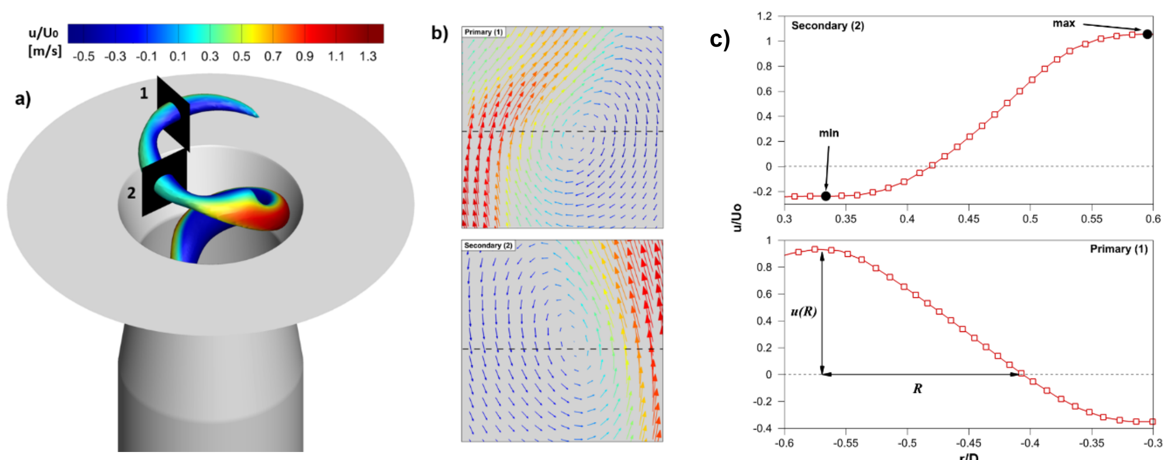


Figure 6. The PVC (a), slices across the PVC (b) and velocity profiles across the slices (c)

## 5 Conclusions

The present study focused on DES computations of isothermal flow fields in premixed vortex burner under unconfined conditions. The burner is operated with air at atmospheric pressure and under high swirl number Sn = 1.05. The multi-block technique is used to generate a structured grid of the vortex burner. The flow fields are characterized using streamline patters colored by axial velocity. The applied DES strategy is useful to capture the averaged flow field with CRZ and ORZ, as well as the specific features of the instantaneous flow filed such as the vortices and the stagnation points in the ISL. PVC is detected in the shear layer of the CRZ. The DES results are found to be in good agreement with experimental data. A phase-angle analysis of the instantaneous flow field show that the PVC further induces unsteady stagnation points. The motion of the stagnation points is linked to the periodic precession of the PVC. The PVC is formed from the contraction to the burner exit and taking on a helical shape. Vectors of the flow fields in two slices across the vortex axis are presented. The circumferential velocity profiles of the vortex centerlines show that the vortex is characterized by the limits of its circumferential velocity u(R) and its corresponding radius R.

## References

[1] Syred N. (2006). A review of instability and oscillation mechanisms in swirl combustion systems. Prog. Energy. Combust. Sci. 32, pp. 93–161.

[2] Galley D, Ducruix S, Lacas F, Veynante D. (2011). Mixing and stabilization study of a partially premixed swirling flame using laser induced fluorescence. Combust. Flame. 158, pp.155–171.

[3] Stöhr M, Boxx I, Carter CD, Meier W. (2012). Experimental study of vortex-flame interaction in a gas turbine model combustor. Combust. Flame. 159, pp. 2636–2649.

[4] Steinberg AM, Arndt CM, Meier W. (2013). Parametric study of vortex structures and their dynamics in swirl-stabilized combustion. Proc. Combust. Inst. 34, pp. 3117–3125.

[5] Fernandes EC, Heitor MV, Shtork SI. (2006). An analysis of unsteady highly turbulent swirling flow in a model vortex combustor. Exp. Fluids. 40, pp. 177–187.

[6] Fureby C, Grinstein FF, Li G, Gutmark EJ. (2007). An experimental and computational study of a multi-swirl gas turbine combustor. Proc. Combust. Inst. 31, pp. 3107–3114.

[7] Legrand M, Nogueira J, Lecuona A, Nauri S, Rodriguez PA. (2010). Atmospheric low swirl burner flow characterization with stereo PIV. Exp. Fluids. 48, pp. 901–913.

[8] Bulat G, Jones WP, Navarro-Martinez S. (2015). Large eddy simulations of isothermal confined swirling flow in an industrial gas-turbine. Int. J. Heat. Fluid. Fl. 51, pp. 50–64.

[9] Zhang H, Han C, Ye T, Zhang J, Chen Y. (2015). Large eddy simulation of unconfined turbulent swirling flow. Sci. China. Technol. Sci. 58, pp. 1731–1744.

[10] Roux S, Lartigue G, Poinsot T, Meier U, Bérat C. (2005). Studies of mean and unsteady flow in a swirled combustor using experiments, acoustic analysis, and large eddy simulations. Combust. Flame. 141, pp. 40–54.

[11] Anacleto PM, Heitor MV. (2001). A laser doppler analysis of the impact of flow boundary conditions on the performance of a model lean premixed combustor. 10th International Symposium on Application of Laser Techniques to Fluid Mechanics, Lisbon, Portugal.

[12] Menter FR. (1994). Two-equation eddy-viscosity turbulence models for engineering applications, AIAA J. 32, pp. 1598-1605.

[13] Strelets M. (2001). Detached Eddy Simulation of massively Separated flows. 39th AIAA Aerospace Sciences Meeting and Exhibit, Reno NV, USA.

[14] Mansouri Z, Aouissi M, Boushaki T. (2016). Detached Eddy Simulation of High Turbulent Swirling Reacting Flow in a Premixed Model Burner, Combust. Sci. Technol. 188, pp. 1777–1798.